Reduction of the glass transition temperature in polymer films: A molecular-dynamics study

F. Varnik,[1,*] J. Baschnagel,[2] and K. Binder[1]
[1]*Institut für Physik, Johannes-Gutenberg Universität, D-55099 Mainz, Germany*
[2]*Institut Charles Sadron, 6 rue Boussingault, F-67083, Strasbourg Cedex, France*
(Received 15 June 2001; published 23 January 2002)

We present results of molecular-dynamics simulations for a nonentangled polymer melt confined between two completely smooth and repulsive walls, interacting with inner particles via the potential $U_{\rm wall}=(\sigma/z)^9$, where $z=|z_{\rm particle}-z_{\rm wall}$ and σ is (roughly) the monomer diameter. The influence of this confinement on the dynamic behavior of the melt is studied for various film thicknesses (wall-to-wall separations) D, ranging from about 3 to about 14 times the bulk radius of gyration. A comparison of the mean-square displacements in the film and in the bulk shows an acceleration of the dynamics due to the presence of the walls. This leads to a reduction of the critical temperature T_c of the mode coupling theory with decreasing film thickness. Analyzing the same data by the Vogel-Fulcher-Tammann (VFT) equation, we also estimate the VFT temperature $T_0(D)$. The ratio $T_0(D)/T_0^{\rm bulk}$ decreases for smaller D similarly to $T_c(D)/T_c^{\rm bulk}$. These results are in qualitative agreement with that of the glass transition temperature observed in some experiments on supported polymer films.

DOI: 10.1103/PhysRevE.65.021507 PACS number(s): 64.70.Pf, 61.20.Ja, 61.25.Hq

I. INTRODUCTION

Polymer science has had a major impact on the way we live. Just 50 years ago, materials we now take for granted were nonexistent. Due to their structural complexity, polymers are generally not crystalline at low temperatures. Rather, they exhibit an amorphous, glassy structure. The concept of the glass transition thus plays an important role in understanding the properties of polymer systems. Polymers are often used as protective coatings in microelectronics [1–3]. In such applications, the polymer is confined in a film geometry. An important information for materials design is, therefore, how thermal properties of a polymer system are affected by the film geometry, in particular, whether and how the glass transition temperature T_g is influenced by confinement.

In addition to its technological importance, the investigation of the glass transition in thin polymer films is also of a great theoretical interest. This is closely related to the unresolved nature of the glass transition. Despite considerable experimental and theoretical efforts, there is still not a fully satisfactory description of this phenomenon. Phenomenological theories of the glass transition, such as the free-volume theory [4–7], are attractive as they give a simple description of the basic observations but they contain adjustable parameters whose physical significance is unclear. Thermodynamic approach, e.g., Gibbs-DiMarzio theory [8,9], treats the glass transition as an ordinary thermodynamic phase transition. The Gibbs-DiMarzio theory implies that the configurational entropy is strictly zero in the glassy phase. However, there are, e.g., two level systems present in the glassy phase, which also contribute to the configurational entropy and not to phonons. Thus, the assumption of vanishing configurational entropy at the glass transition point does not hold for all classes of glassy systems.

The so-called mode coupling theory (MCT) is perhaps the most successful of all descriptions of the glass transition. Within the idealized version of this theory, there is a critical temperature T_c at which the (structural) relaxation times diverge while the static properties of the system remain liquid-like. The system freezes at T_c keeping its amorphous structure. Thus, from the point of view of the MCT, the glass transition is a purely dynamic phenomenon [10–14].

However, it must be stressed that neither MCT nor other descriptions of the glass transition have a definitive character. One is, therefore, interested in finding ways to verify the basic concepts of different approaches.

Let us assume that the slowing down of the dynamics when approaching T_g can be interpreted in terms of the critical slowing down of the dynamics near a second-order phase transition [15]. A second-order phase transition is usually characterized by the divergence of a length scale. The idea of a diverging length scale related to the glass transition has given rise to the concept of ''cooperative motion'' empirically introduced by Adam and Gibbs [16]. According to Adam and Gibbs, near the glass transition, individual particle motion is frozen out. Thus, the only possibility for structural relaxation is that of the collective motion of many particles. Note that, here, the focus is no longer on the static correlations, but on correlations, between the *dynamics* of particles. The associated length scale is thus a dynamic one. Let $\xi(T)$ denote the typical size of a cluster of cooperatively moving particles. It is well known that close to a second-order phase transition the relaxation time of such a cluster scales as ξ^z, where $z>0$ is the so-called dynamic critical exponent [17]. The sharp rise of the relaxation times near T_g is then explained by assuming the divergence of ξ when lowering the temperature towards T_g.

The above reasoning, however, is based on an empirical assumption that $\xi(T)$ increases with decreasing temperature. A significant improvement was achieved by Edwards and Vilgis [18]. These authors introduced an exactly solvable model system exhibiting glassy behavior at low T and

*Corresponding author. Email address: varnik@mail.uni-mainz.de

showed that the concept of cooperative motion alone was enough to give rise to a Vogel-Fulcher-Tammann (VFT) law.

Recent computer experiments also support the idea of cooperative motion. For example, it was observed by Kob and co-workers [19,20] that particles move mainly in stringlike clusters. Bennemann *et al.* [21] report on a growing length scale for the dynamics of a polymer melt. A strong heterogeneity in the dynamics has also been observed in molecular-dynamics simulations of bond breakage processes [22] and of binary mixture of soft spheres [23–25]. It is found that the particles move preferably within mobile clusters thus leading to a heterogeneity in the dynamics.

While easily detectable in a simulation, the regions of heterogeneous dynamics are unfortunately not as easily accessible to real experiments. This results from the fact that dynamic heterogeneity is not necessarily strongly correlated to density fluctuations. The structures of these regions are, therefore, more or less identical. Thus, one cannot use scattering experiments to determine the length scale $\xi(T)$ [26]. Fortunately, there is a clue to this problem. Recall that the relaxation time of a cluster of strongly correlated particles, such as that observed in cooperative motion scales like ξ^z, where $z>0$. As the temperature decreases, $\xi(T)$ becomes larger and eventually reaches the system size $\xi(T)=L$. If this occurs, the relaxation time τ of the system will scale as $\tau \propto L^z$. In other words, the relaxation dynamics of the system will become size dependent. This size dependence is indeed observed in Monte Carlo studies of the so-called bond-fluctuation model (BFM) in two-dimensions [27]. In the mentioned reference, the system size was varied while maintaining the periodic boundary conditions. An acceleration of the dynamics of the smaller systems has been observed in accordance with $\tau \propto L^z$.

A simple way of changing the system size in a real experiment is, for example, to vary the thickness of a planar film. Applying the same arguments as given above to a thin film of thickness D we should expect finite-size effects on the dynamics for temperatures at which $\xi(T) \approx D$. Note that boundary conditions are no longer periodic, but can change from an absorbing one to an approximately neutral or a repulsive one.

In this context, experiments on (model) systems reveal mixed findings. If the interaction between the polymers and the substrate is attractive, the glass transition temperature T_g of the films becomes larger than the bulk value for small film thicknesses [28]. Intuitively, this effect can be attributed to chains that are close enough to the substrate to ''feel'' the attractive interaction. The motion of these chains should be slowed down with respect to the bulk. In a thin film almost all chains touch the attractive substrate. So, T_g should increase.

On the other hand, measurements (by ellipsometry) of T_g for polystyrene films (of rather large molecular weights) on a silicon substrate showed a significant decrease of T_g from 375 K down to 345 K for the smallest film thickness of 10 nm, i.e., a relative change of 10% in T_g was observed [29]. There have also been many experiments in recent years on freely standing polystyrene films (i.e., no solid substrate, but two polymer-air interfaces) [30–33] showing a dramatic decrease of T_g by up to 20% if the film thickness becomes much smaller than the chain size. An interesting explanation of this observation in terms of an interplay between polymer-specific properties and free-volume concepts has been proposed [34]. This decrease becomes much weaker if one or even both of the free interfaces are replaced by a weakly interacting solid substrate. Whereas the strong depression of T_g in the freely standing film could possibly be attributed to the significant release of geometric constraints at the air-polymer interface, the acceleration of the structural relaxation of a polymer melt between two (almost) neutral solid substrates is much harder to understand intuitively.

Recent simulation results emphasize the fact that the increase or decrease of the glass transition temperature does strongly depend on the interaction between the polymer chains and the substrate [35]. For a model of square-well spherical interaction sites interconnected by fully flexible strings, one observes a reduction of T_g in the case of a weak attraction between the substrate and the chains, whereas for the case of strong attraction an increase of T_g is found [35].

We study a continuum model where polymer chains are confined between two identical, ideally flat and purely repulsive walls [36,37], obtaining complete information in both space and time in atomistic detail. Instead of focusing on a computation of T_g, we rather check some predictions of the mode coupling theory and investigate the dependence of the mode coupling critical temperature T_c on film thickness D. We also examine the D dependence of the VFT temperature T_0 with the result that the ratios $T_0(D)/T_0^{\text{bulk}}$ and $T_c(D)/T_c^{\text{bulk}}$ behave similarly.

After a presentation of the model in the following section, we discuss in Sec. III the reliability of the system dynamics obtained from molecular-dynamics (MD) simulations within *NVT* and *NpT* ensembles. In Sec. IV we present MD results on the influence of the walls on the system mobility and its critical behavior at low temperatures for a variety of film thicknesses showing that the critical temperature is lowered for stronger confinements (smaller film thicknesses). Section V is devoted to a brief analysis of the local dynamics where we address a subtle point concerning the proper definition of local quantities in terms of particle positions and/or momenta. A conclusion compiles the results.

II. MODEL

We study a Lennard-Jones (LJ) model for a dense polymer melt [38,39] of short chains (each consisting of 10 monomers) embedded between two completely smooth, impenetrable walls [36,37]. Two potentials are used for the interaction between particles. The first one is a truncated and shifted LJ potential, which acts between all pairs of particles regardless of whether they are connected or not,

$$U_{\text{LJ-ts}}(r)=\begin{cases} U_{\text{LJ}}(r)-U_{\text{LJ}}(r_c) & \text{if } r<r_c \\ 0 & \text{otherwise} \end{cases}$$

where $U_{\text{LJ}}(r)=4\epsilon[(\sigma/r)^{12}-(\sigma/r)^6]$ and $r_c=2\times 2^{1/6}\sigma$. The connectivity between adjacent monomers of a chain is ensured by a FENE potential [38]

$$U_{\mathrm{FENE}}(r) = -\frac{k}{2} R_0^2 \ln\left[1 - \left(\frac{r}{R_0}\right)^2\right], \tag{1}$$

where $k = 30\epsilon/\sigma^2$ is the strength factor and $R_0 = 1.5\sigma$ the maximum allowed length of a bond. The wall potential was chosen as

$$U_W(z) = \epsilon\left(\frac{\sigma}{z}\right)^9. \tag{2}$$

where $z = |z_{\mathrm{particle}} - z_{\mathrm{wall}}|$ ($z_{\mathrm{wall}} = \pm D/2$). This corresponds to an infinitely thick wall made of infinitely small particles that interact with inner particles via the potential $45\epsilon(\sigma/r)^{12}/(4\pi\rho_{\mathrm{wall}}\sigma^3)$, where ρ_{wall} denotes the density of wall particles. The sum over the wall particles then yields $\epsilon(\sigma/z)^9$. All simulation results are given in LJ units. Lengths and energies are measured, respectively, in units of σ and ϵ, temperature in units of ϵ/k_B ($k_B = 1$), time in units of $(m\sigma^2/\epsilon)^{1/2}$ ($m = 1$) and pressure in units of ϵ/σ^3.

The upper panel of Fig. 1 compares the bond potential, i.e., the sum of LJ and FENE potentials, with the LJ potential. It shows that the bonded monomers prefer shorter distances than the nonbonded ones. Thus, our model contains two intrinsic length scales. Since these length scales are chosen to be incompatible with a (fcc or bcc) crystalline structure, one could expect that the system does not crystallize at low temperatures, but remains amorphous. This expectation is well borne out. The lower panel of Fig. 1 compares the structure factor $S(q)$ of the bulk system with that of a film of thickness $D = 10$ at $T = 0.46$ (note that the mode coupling critical temperature of the present model in the bulk is $T_c^{\mathrm{bulk}} = 0.45$ [40]). For the film, two structure factors are chosen, corresponding to two different regions: a layer of thickness 3σ centered in the middle of the film (called ''film center'') and the region between this layer and the walls (called ''near walls''). In both cases, $S(q)$ is calculated parallel to the walls [i.e., $q = |q|$, $\mathbf{q} = (q_x, q_y)$] by averaging over all monomers in the respective region.

The lower panel of Fig. 1 shows that the structure of the melt in the bulk and in the film is characteristic of an amorphous material. At small q, $S(q)$ is small, reflecting the low compressibility of the system. Then, it increases and develops a peak at q_{max}, which corresponds to the local packing of monomers ($2\pi/q_{\mathrm{max}} \approx 1$) before it decreases again and begins oscillating around 1, the large-q limit of $S(q)$.

The most prominent differences between the bulk and the film are found for small q and for q_{max}. The compressibility of the film is higher, the value of q_{max} is shifted to slightly lower q and the magnitude of $S(q_{\mathrm{max}})$ is smaller than in the bulk. In the bulk one can observe a similar shift of q_{max} and decrease of $S(q_{\mathrm{max}})$ as the temperature increases. Also the compressibility of a bulk fluid increases with temperatures. Therefore, the local packing of the monomers in the film seems to resemble that of the bulk at a higher temperature. Since the local structure of the melt has an important influence on its dynamic behavior in the supercooled state [11], the lower panel of Fig. 1 suggests that the film relaxes more easily than the bulk at the same temperature. Indeed, we will see later that the dynamics of the system is much faster in the film than in the bulk when compared at the same temperature.

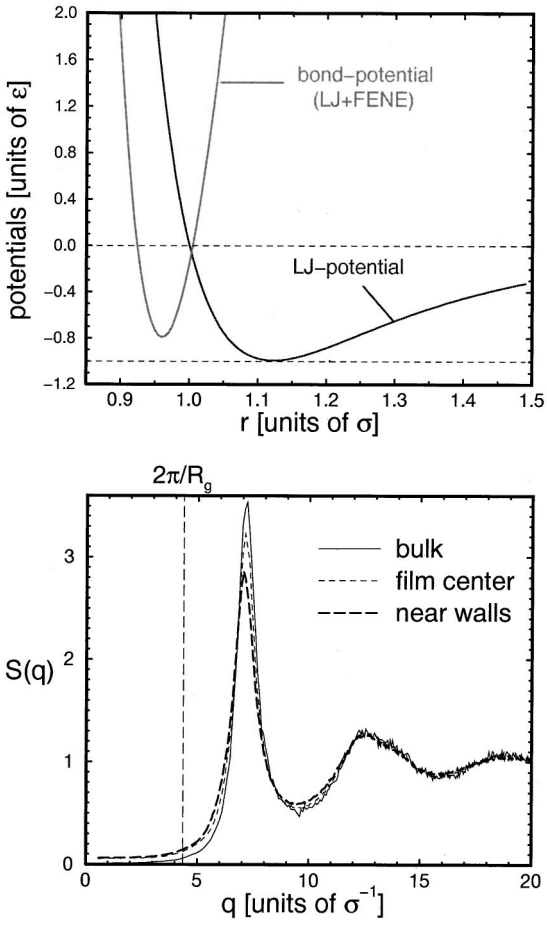

FIG. 1. Upper panel: Illustration of the potentials of the model. The bond-potential results from a superposition of the Lennard-Jones (LJ) and the FENE potentials. The minimum position of the bond potential is smaller than that of the LJ potential. This incompatibility favors amorphous structure at low T, which is confirmed by the behavior of $S(q)$. Lower panel: Comparison of the static structure factor $S(q)$ of the melt in the bulk and in the film ($D = 10$) at $T = 0.46$ (critical temperature of mode coupling theory in the bulk: $T_c \simeq 0.45$ [40]). ''Near walls'' and ''film center'' mean averages over the regions close to the walls ($0 \leqslant z \leqslant 3.5$) and the inner portion of the film ($3.5 \leqslant z \leqslant 5$). z is the distance of a particle from the (left) wall. The vertical dashed line indicates the q value corresponding to the bulk radius of gyration ($R_g^2 \simeq 2.09$).

All simulations have been carried out under constant normal pressure $P_{N,\mathrm{ext}} = p = 1$. However, to adjust the normal pressure, we do *not* vary the wall-to-wall separation D, but the surface area. For each temperature, the average surface area is calculated by an iterative approach [41]. The system is then propagated until the instantaneous surface area reaches the computed average value. At this point the surface area (and thus the volume) is fixed and a production run is started in *NVT* ensemble, where the system temperature is adjusted using the Nosé-Hoover thermostat [42,43]. More details about the applied simulation techniques can be found in [37,41,44].

III. *NVT* AND *NpT* VERSUS *NVE*: INFLUENCE ON THE DYNAMICS

It was mentioned in Sec. II that the production runs were performed at a constant volume and temperature using Nosé-Hoover thermostat. This thermostat slows down or accelerates all particles depending on the sign of the difference between the instantaneous kinetic energy of the system and the desired value given by the imposed temperature, i.e., $3Nk_BT/2$ (N is the number of particles) [42,43,45–48]. One may therefore ask how reliable the resulting dynamics is when compared to pure Newtonian dynamics in the microcanonical (*NVE*) ensemble. This question was already examined for the bulk system in [39]. In this case, the results obtained within constant energy (*NVE*) simulation and that using the Nosé-Hoover thermostat are identical.

We are going to show that the presence of the walls does not change this behavior. However, we go a step further and also investigate the influence of volume fluctuations on the system dynamics. This point is very important if one is interested in constant pressure simulations. We will see that, contrary to the case of Nosé-Hoover thermostat, the system dynamics is strongly perturbed when the system volume is allowed to fluctuate (therefore, for a given normal pressure, the corresponding average volume was first computed for each T in a *NpT* simulation and then the dynamics was analyzed in production runs at a constant volume). For this purpose, we compare results obtained from MD simulations within the *NVE* (microcanonical). *NVT* (canonical, using Nosé-Hoover thermostat) and *NpT* (Nosé-Hoover thermostat plus the fluctuations of the surface area) ensembles.

Note that all results to be discussed in this section correspond to a film of thickness $D=5$. Recall that D stands for the wall-to-wall separation. The distance of the closest approach of a monomer to a wall is approximately its own diameter (i.e., $\sigma=1$). Therefore, a value of $D=5$ corresponds to the extreme case of three monomer layers only.

Let us first consider the velocity autocorrelation function defined as

$$C_v(t)=\left\langle \sum_i^N \mathbf{v}_i(0)\cdot\mathbf{v}_i(t)\right\rangle \Big/ \left\langle \sum_{i=1}^N v_i^2(0)\right\rangle. \qquad (3)$$

Figure 2 presents results for $C_v(t)$ obtained from simulations in the *NVE*, *NVT*, and *NpT* ensembles. As seen from this figure, no difference is observed for $C_v(t)$ within various ensembles. The velocity autocorrelation function vanishes so rapidly that it can be equally well computed within all these ensembles. However, quantities that evolve slowly in time exhibit a different behavior. An example is the mean-square displacement (MSD) of chain's center of mass

$$g_{3,\|}(t)=\frac{1}{M}\sum_{i=1}^M \langle[\mathbf{R}_{\mathrm{cm},i,\|}(t)-\mathbf{R}_{\mathrm{cm},i,\|}]^2\rangle. \qquad (4)$$

Here, M is the number of chains and $R_{cm,i,\|}$ is the projection of the center of mass vector of the ith chain onto a plane parallel to the wall. Figure 3 shows that data for $g_{3,\|}(t)$ within *NVE* and *NVT* ensembles are identical. However, the result obtained from the *NpT*-ensemble differs strongly from the reference *NVE* curve. This discrepancy is due to the relative small box size of a typical MD simulation. Note that the relative volume fluctuations scale as $1/\sqrt{N}$. While fully negligible for real systems ($N\approx 10^{23}$), these fluctuations become important in a simulation where the particle number is of order of 1000.

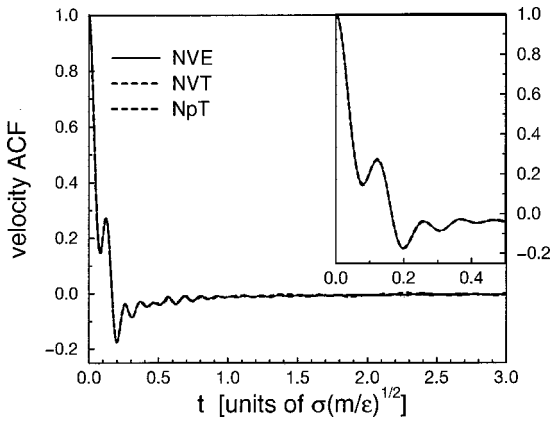

FIG. 2. Velocity autocorrelation function (ACF) as computed from simulation runs within the *NVE*, *NVT*, and *NpT* ensembles. Neither the coupling to the heat bath nor the fluctuations of the volume seem to affect the behavior of this quantity. The inset shows a magnification of the initial behavior of the velocity ACF ($D=5$, $P_N=1$, $T=0.55$, $N=500$).

IV. DEPENDENCE OF T_c ON FILM THICKNESS

We now focus on the influence of the walls on the sluggish dynamics of the system. For this purpose, it is instructive to recall some important features of the present model in the bulk at low temperatures. In Fig. 4 the mean-square displacements of the innermost monomer

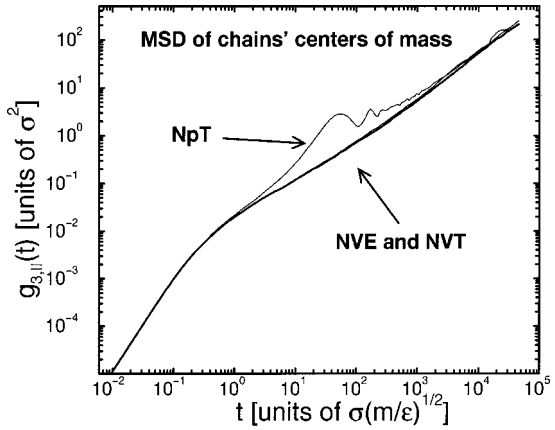

FIG. 3. The mean-square displacement (MSD) of chain's center of mass in the direction parallel to the walls, $g_{3,\|}(t)$, obtained from *NVE*, *NVT*, and *NpT* simulation runs ($D=5$, $P_N=1$, $T=0.55$, $N=500$). Obviously, the *NVT* result is identical to that obtained within the *NVE*-ensemble simulation. Contrary to that, the time evolution of $g_{3,\|}(t)$ in the *NpT*-ensemble simulation is unphysical for $t\geqslant 1$.

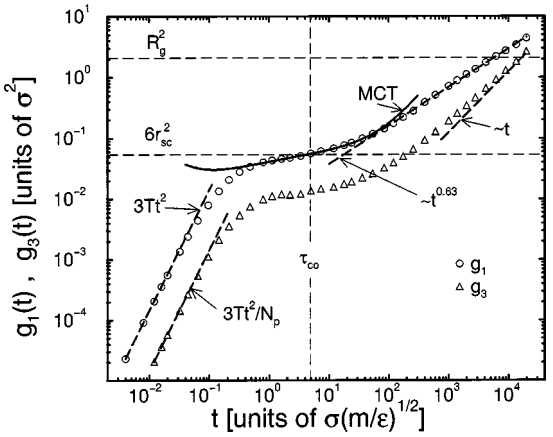

FIG. 4. Log-log plot of the mean-square displacements of the innermost monomer $g_1(t)$ and of the chain's center of mass $g_3(t)$ versus time for $T=0.48$. The initial ballistic behaviors for $g_1(t)$ and $g_3(t)$, i.e., $g_1(t)=\langle v^2\rangle t^2=3Tt^2$ and $g_3(t)=3Tt^2/N_p$ [$\langle v^2\rangle$: mean-square monomer velocity, $N_p=10$: chain length], and the late time diffusive behavior are indicated as dashed lines. In addition, a power law fit $g_1(t)\sim t^x$ with an effective exponent $x\simeq 0.63$ is shown as another dashed line. The dashed horizontal lines represent the radius of gyration R_g^2 ($\simeq 2.09$; upper line) and the plateau value $6r_{sc}^2$ of a MCT analysis ($\simeq 0.054$; lower line), respectively. The dashed vertical line indicates the time τ_{co} of the intersection between $g_1(t)$ and $6r_{sc}^2$. Additionally, the mode coupling approximation in the β-relaxation regime is shown as a thick solid line. Adapted from reference [52].

$$g_1(t)=\frac{1}{M}\sum_{i=1}^{M}\langle[\mathbf{r}_{i,\mathrm{inner}}(t)-\mathbf{r}_{i,\mathrm{inner}}(0)]^2\rangle, \qquad (5)$$

and of the chain's center of mass $g_3(t)$ are displayed versus time for $T=0.48$. For short times, the motion of the system can be described by assuming free particles (ballistic regime): $g_1(t)=\langle v^2\rangle t^2=3Tt^2$ and $g_3(t)=3Tt^2/N_p$, where $\langle v^2\rangle$ is the mean-square monomer velocity and $N_p=10$ is the number of the monomers of a chain. In agreement with the predictions of the MCT [10–14], a plateau regime emerges after the ballistic motion. The tagged particle ''feels'' the presence of its neighbors and, as the temperature is low, remains temporarily in the cage formed by these neighbors. However, contrary to simple (atomic) liquids, where a direct crossover from the plateau into the diffusive regime occurs, an intermediate subdiffusive regime emerges due to the connectivity of the monomers [49]. In this regime, the center of mass already crosses over to the asymptotic diffusive motion, $g_3(t)\simeq t$, whereas the motion of the innermost monomer is described by a power law $g_1(t)\sim t^x$ with an effective exponent $x\simeq 0.63$. The innermost monomers reach the diffusive limit only if $g_1(t)$ is larger than the end-to-end distance of a chain and thus outside of the time window shown in the figure.

In Fig. 5 we compare the mean-square displacement of the innermost monomer $g_1(t)$ for films of various thicknesses with that of the bulk. The upper panel corresponds to a high temperature of $T=1$ where the system properties are liquidlike. At this temperature the influence of the walls is

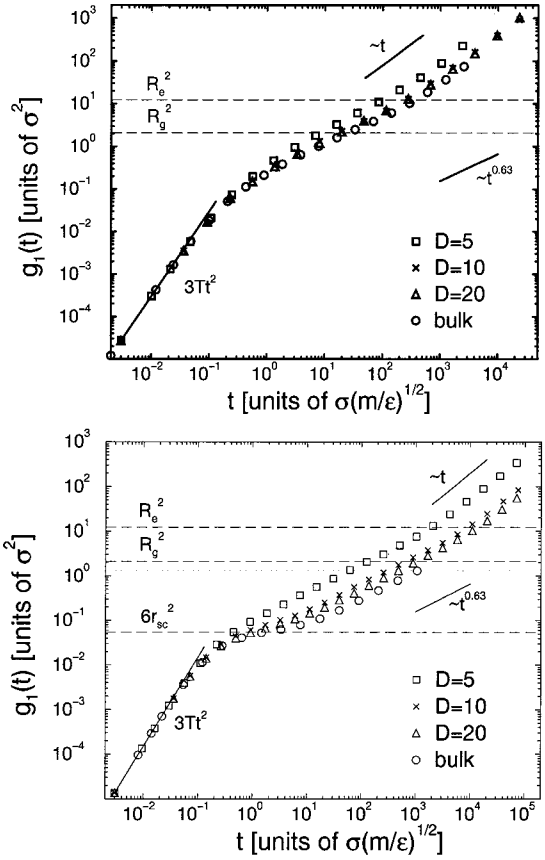

FIG. 5. Log-log plot of the mean-square displacement of the innermost monomer $g_1(t)$ for two different temperatures: $T=1$ (high temperature, normal liquid state; upper panel) and $T=0.5$ (supercooled state close to $T_c^{\mathrm{bulk}}=0.45$; lower panel). The figures compare bulk data with the displacements measured parallel to the walls in films of different thickness: $D=5(\approx 3.5R_g)$, $D=10$ ($\approx 7R_g$) and $D=20(\approx 14R_g)$. The film data were multiplied by $\frac{3}{2}$ to account for the different number of spatial directions used to calculate $g_1(t)$ (i.e., three directions for the bulk, but only two for the films). The bulk end-to-end distance R_c^2 and radius of gyration R_g^2 are indicated as dashed horizontal lines. Furthermore, the lower panel also shows the plateau value $6r_{sc}^2$ of a MCT analysis ($\simeq 0.054$; lowest dashed line). The solid lines represent the behavior of $g_1(t)$ expected in different time regimes: ballistic at short times [$g_1(t)\sim t^2$], diffusive at late times [$g_1(t)\sim t$], and dominated by chain connectivity for times where $g_1(t)>1$ is the monomer diameter [$g_1(t)\sim t^x$; $x=0.63$ is the effective exponent].

rather small so that $g_1(t)$ of the bulk almost overlaps with that of the film for thicknesses $D\geqslant 10$. However, the lower panel of Fig. 5 shows that the effect of the walls on the mobility becomes significant at all studied film thickness with progressive supercooling. Outside the initial ballistic regime, the motion is faster, the smaller the film thickness.

To quantify this observation, we define relaxation times as the time needed by a given mean-square displacement (like g_3, the MSD of chain's center of mass or g_1, the MSD of the innermost monomer) to reach the monomer size

$$g_i(t=\tau):=1 \quad \text{(defining equation for } \tau\text{)}. \qquad (6)$$

TABLE I. Survey of the VFT temperature T_0, mode coupling critical temperature T_c, and the critical exponent γ for different film thicknesses D and for the bulk. T_0 was determined via fits to Eq. (10) both for the film and for the bulk. As to T_c, we determined $T_c(D)$ from fits to Eq. (9). $T_c^{\rm bulk}$ and $\gamma_{\rm bulk}$ were known from previous analyses [39,40,50,51]. This results for $T_c^{\rm bulk}$ is also obtained applying Eq. (9) to the bulk data.

D	5	7	10	15	20	Bulk
T_0	0.204 ± 0.007	0.253 ± 0.013	0.288 ± 0.006	0.297 ± 0.007	0.308 ± 0.004	0.328 ± 0.008
T_c	0.305 ± 0.006	0.365 ± 0.007	0.390 ± 0.005	0.405 ± 0.008	0.415 ± 0.005	0.450 ± 0.005
γ	2.5 ± 0.2	2.4 ± 0.2	2.1 ± 0.1	2.2 ± 0.1	2.1 ± 0.1	1.95 ± 0.1

Note that, due to the film geometry, there are only two independent directions (each of them parallel to the walls) for diffusive motion compared with three in a homogeneous melt. For the film, we thus compute g_i using these two directions and then multiply the result by a factor of $\frac{3}{2}$. This multiplication is necessary if the film data are to be compared with the corresponding bulk quantities.

Using Eq. (6), we computed $\tau(g_i=1)$ as a function of the temperature for various film thicknesses, where, in addition to g_3 and g_1, the MSD of all monomers

$$g_0(t)\frac{1}{N}\sum_{i=1}^{N}\langle[\mathbf{r}_i(t)-\mathbf{r}_i(0)]^2\rangle, \tag{7}$$

and that of the end monomers (chain ends)

$$g_4(t)=\frac{1}{M}\sum_{i=1}^{M}\langle[\mathbf{r}_{i,\rm end}(t)-\mathbf{r}_{,\rm end}(0)]^2\rangle, \tag{8}$$

have also been used.

For each film thickness, this yields four different relaxation times as a function of the temperature. As the mode coupling theory [10–14] has been rather successful in describing the slow dynamics of the present model in bulk [40,50,51], we tried to fit $\tau(T)$ via a power law

$$\tau(T)\propto[T-T_c(D)]^{-\gamma(D)}. \tag{9}$$

Such a power-law divergence of the α-relaxation time is predicted by the MCT for the bulk [11,12,14].

The fit is done as follows: First, all (three) parameters of Eq. (9) were adjusted. The values of γ obtained from $\tau(g_0=1)$, $\tau(g_1=1)$, $\tau(g_3=1)$, and $\tau(g_4=1)$ agreed well within the error bars. Therefore, we fixed γ at the average value for the given film thickness and repeated the fits.

Table I contains results for $T_c(D)$ and $\gamma(D)$ obtained in this way. Figure 6 shows a representative example for this analysis. It depicts $\tau^{-1/\gamma}$ versus T for a film of thickness $D=5$ (note that D is the wall-to-wall distance, the thickness of the region with nonvanishing monomer density is approximately $D-2$, see Fig. 19). The intersection of the straight lines (MCT -fit results) with the T axis yields the critical temperature at this film thickness: $T_c(D=5)=0.305\pm0.005$. Note that, despite the highly nonlinear relationship between the MSD's used to define the various τ's all fits yield the same T_c.

To test this analysis the resulting critical temperature can be used to linearize reduced plots of the relaxation times versus $T-T_c$ on a log-log scale. Figures 7 and 8 show that the power law (9) motivated by the ideal MCT is a good approximation of the data at temperatures close (but not too close) to T_c (see, for example, Fig. 10 and also [40,50,52] for comparable bulk data).

However, as indicated by the solid line in the both figures, $\tau(T)$ can also be described by a VFT fit in the studied temperature range, i.e., by

$$\tau(T)\propto\exp\left(\frac{c(D)}{T-T_0(D)}\right), \tag{10}$$

where c is a constant, which can depend on film thickness. The possibility of describing the same data both by a power law (MCT) and by a VFT fit has also been observed for bulk properties of the present model (see Fig. 10 in [39]). We therefore use the VFT formula as an independent approach and determine the VFT temperature T_0 for various film thicknesses. Table I contains the results for $T_0(D)$ thus obtained. A plot of $T_c(D)/T_c^{\rm bulk}$ and $T_0(D)/T_0^{\rm bulk}$ is shown in Fig. 9. Both the mode coupling critical temperature and the VFT temperature exhibit similar D dependences, thus suggesting that the presence of the smooth walls results in a

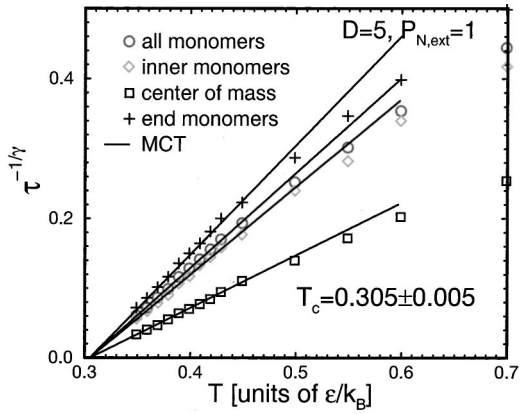

FIG. 6. Plot of $\tau^{-1/\gamma}$ versus T the relaxation time τ [measured in units of $\sigma(m/\epsilon)^{1/2}$] was determined by Eq. (6) using the mean-square displacements of inner, end, and all monomers and of the chain's center of mass. The mode coupling exponent γ was first determined from fits to Eq. (9) where all fit parameters were first treated as independent. As all values obtained for γ agreed within the error bars, $\gamma=2.5\pm0.2$, we repeated the fits with $\gamma=2.5$. The MCT fits to the data are represented by the straight lines. From the intersection of these lines with the T axis the critical temperature is determined $T_c(D=5)=0.305\pm0.005$.

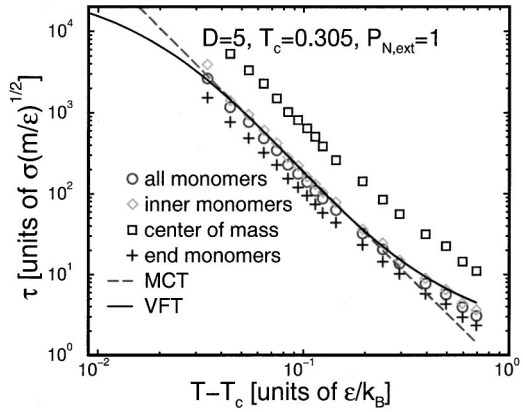

FIG. 7. Relaxation time $\tau(g_i=1)$ for an extremely thin film of three monomer layers only (wall-to-wall distance $D=5$). Different mean-square displacements are used for the analysis: g_0 is the MSD of all monomers, g_1 is the MSD of the innermost monomer, g_3 is the MSD of the chain's center of mass, and g_4 is the MSD of the end monomers. The long-dashed line indicates the fit using Eq. (9) motivated by the ideal mode coupling theory. However, the solid line that corresponds to a fit using the VFT law describes equally well the data [see Eq. (10)]. Both fits shown here were done for $g_1(t)$.

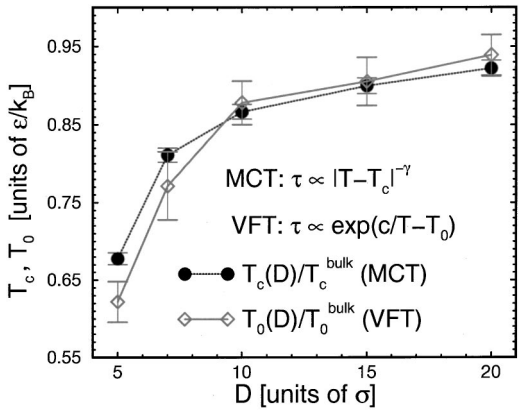

FIG. 9. Ratios $T_c(D)/T_c^{\mathrm{bulk}}$ and $T_0(D)/T_0^{\mathrm{bulk}}$ versus film thickness D. The critical temperatures $T_c(D)$ of the films were obtained from fits to Eq. (9). Similarly, the Vogel-Fulcher-Tammann temperatures $T_0(D)$ and T_0^{bulk} are results of fits to Eq. (10). The error bars of $T_0(D)$ are larger than those of $T_c(D)$, since $T_0(D) \ll T_c(D)$ so that the difference between the lowest simulated temperature and the extrapolated result is much larger for the VFT temperature than for the critical temperature. Therefore, the results for $T_c(D)$ are more reliable.

reduction of the glass transition temperature T_g. As already mentioned in Sec. I a reduction of the glass transition temperatures has also been reported both from experiments on supported polymer films [29] and on free-standing polymer films [26,31,53] and also from MD simulations of a model of square-well spherical interaction sites interconnected by fully flexible strings in the case of a weak attraction between the substrate and the chains [35].

In Fig. 10, $\tau(g_1=1)$ is depicted versus $T-T_c$ for the homogeneous melt (bulk) and films of various thicknesses. The solid line indicates the power law $\tau \sim (T-T_c^{\mathrm{bulk}})^{-\gamma_{\mathrm{bulk}}}$ with $T_c^{\mathrm{bulk}}=0.45$ and $\gamma_{\mathrm{bulk}}=1.95$. The value of γ_{bulk} used here corresponds to that obtained from a similar power law fit to the (bulk) self-diffusion coefficient [39].

To show the (slight) D dependence of the exponent γ, a fit to $D=5$ data is also depicted (see the long-dashed line with an slope of 2.5). It is seen from this figure that both in the film and in the bulk, for temperatures very close to T_c, the relaxation times increase more slowly than predicted by the ideal MCT. This discrepancy is an indication of slow relaxation processes that are not taken into account within the ideal MCT. As temperature decreases, the contribution of these processes becomes important and the ideal MCT no

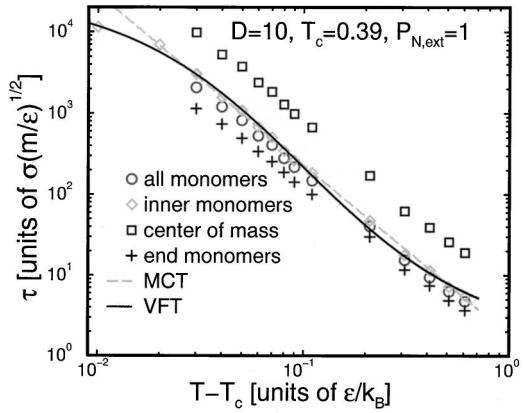

FIG. 8. Relaxation time $\tau(g_i=1)$ for a film of thickness $D=10$. Different mean-square displacements are used for the analysis: g_0 is MSD of all monomers, g_1 is the MSD of the innermost monomer, g_3 is the MSD of the chain's center of mass, and g_4 is the MSD of the end monomers. The long-dashed line indicates the fit using Eq. (9) motivated by the ideal mode coupling theory. The solid line corresponds to a fit using the VFT law [see Eq. (10)]. Both fits shown here were done for $g_1(t)$.

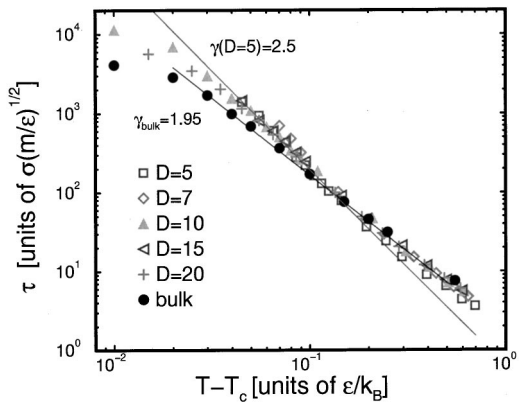

FIG. 10. Relaxation time τ determined from $g_1(t)$ by requiring $g_1(\tau)=1$ (being monomer diameter). The solid line indicates the power law $\tau \sim (T-T_c^{\mathrm{bulk}})^{-\mathrm{bulk}}$ suggested by MCT for the bulk at temperatures above T_c^{bulk} ($T_c^{\mathrm{bulk}}=0.45$ and $\gamma_{\mathrm{bulk}}=1.95$ [39]). The long-dashed line represents a fit to $D=5$ data with an exponent of $\gamma(D=5)=2.5$. Both in the film and in the bulk, for temperatures very close to T_c, the relaxation times increase more slowly than predicted by the ideal MCT.

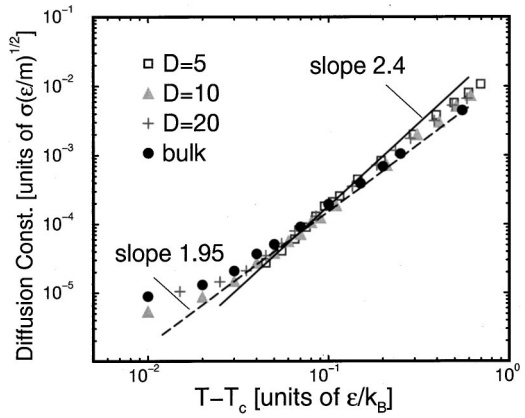

FIG. 11. Diffusion constant of a chain versus $T-T_c$ for films of thickness $D=5$, 10, 20, and for the bulk. The critical temperatures $T_c(D)$ of the films were obtained from fits to Eq. (9) [see Table I]. T_c^{bulk} was known from the previous bulk analysis [40]. The straight lines indicate fits using Eq. (12). The mode coupling exponent γ is larger for stronger confinement (smaller film thickness). Note that, the lowest simulated temperature is $T=0.35$ for $D=5$ and $T=0.4$ for $D=10$. However, as the critical temperature of the thinner film is much lower [$T_c(D=5)=0.305$ compared to $T_c(D=10)=0.39$] the $D=10$ data are *closer* to the corresponding T_c. This explains why practically no deviation from a power law is observed for $D=5$.

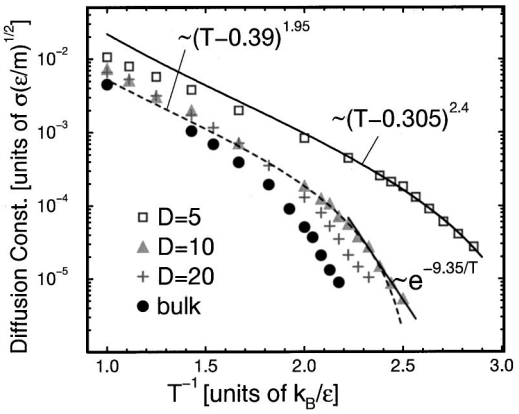

FIG. 12. Diffusion constant of a chain versus inverse temperature for films of thickness $D=5$, 10, 20, and for the bulk. The critical temperatures $T_c(D)$ of the films were obtained from fits to Eq. (9) [see Table I]. T_c^{bulk} was known from the previous bulk analysis [40]. The solid line indicates the fit results using Eq. (12) for $D=5$. The dashed line indicates a similar fit result for $D=10$. A short solid line indicates the result of an Arrhenius fit [see Eq. (11)] to the $D=10$ data in a low temperature range, where the ideal MCT no longer holds [see also the text]. Note that, the lowest simulated temperature is $T=0.35$ for $D=5$ and $T=0.4$ for $D=10$. However, as the critical temperature of the thinner film is much lower [$T_c(D=5)=0.305$ compared to $T_c(D=10)=0.39$], the $D=5$ data are *farther* from the corresponding T_c. This explains why a power law fits well to $D=5$ data at all temperatures.

longer holds. A common picture in describing the slow dynamics of the system at these temperatures is that of an energy landscape with *finite* potential barriers. Relaxation processes are then described as jumps (hoppings) between neighboring energy minima. If one assumes a sharp distribution of the potential barriers around a given value, E_0, i.e., if all such barriers are assumed to have more or less the same height, the probability of a jump over a barrier is then equal to the probability of having an energy $E \geqslant E_0$. Assuming that the diffusion constant $\mathcal{D}$ is proportional to this probability, one obtains

$$\mathcal{D} \propto \int_{E_0}^{\infty} \exp\left(-\frac{E}{k_B T}\right) dE = \exp\left(-\frac{E_0}{k_B T}\right). \tag{11}$$

Thus, due to the above picture, at low enough temperatures the diffusion constant obeys an Arrhenius law. Here, ''low enough'' means temperatures very close to or below T_c. However, for higher (but not too high) temperatures one again expects the validity of a power law also for the diffusion constant

$$\mathcal{D} \propto |T - T_c(D)|^{\gamma(D)}. \tag{12}$$

Using the mean-square displacements, we compute the diffusion constant from

$$\mathcal{D} = \lim_{t\to\infty} \frac{g_i(t)}{6t}. \tag{13}$$

Note that, in the diffusive limit ($t\to\infty$), there is no difference between g_0, g_1, g_3 or g_4 [see, for example, the upper panel in Fig. 14, where $g_0(t)$ and $g_3(t)$ coincide for large t]. In the praxis, however, one has to evaluate Eq. (13) at large but finite t. As the mean-square displacements of chain's center of mass reaches the diffusive limit faster than other MSD's (see Fig. 4), one should use $g_3(t)$ in an evaluation of Eq. (13).

The best results on the diffusion constant one obtains are numerical. A log-log plot of the diffusion constant versus $T-T_c$ is depicted in Fig. 11 for various film thicknesses and for the bulk. Similar to the behavior of the relaxation time discussed above, at temperatures very close to T_c, results for the diffusion constant deviate from the power law given by Eq. (12). Motivated by the discussion that led to Eq. (11), we try to fit the diffusion constant at law temperatures by an Arrhenius law. This is demonstrated in Fig. 12 for the case of a film of thickness $D=10$, where Eq. (11) is applied to the last few data points in low temperature regime. From this fit, we obtain $E_0 \approx 9.35$. However, one should be careful with an interpretation of E_0. Recall that Eq. (11) was derived assuming that all potential barriers have the same height of E_0. Therefore, an interpretation of E_0 as the typical height of the potential barriers in an energy landscape requires a study of the inherent structure of the system.

It is also shown in Fig. 12 that the data at higher but not too high temperatures are well described by a power law, as expected from the MCT analysis of the relaxation times presented in this section.

Next we look at the temperature dependence of a crossover time τ_{co} given by

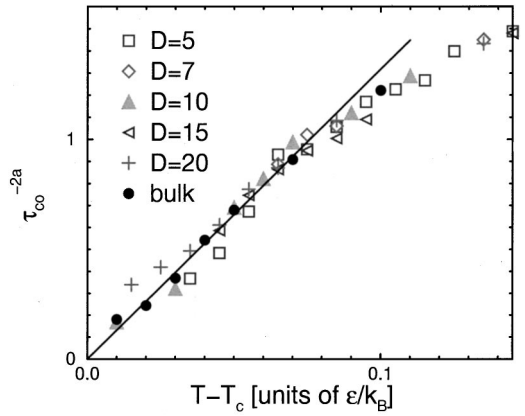

FIG. 13. Temperature dependence of the crossover time τ_{co} [measured in units of $\sigma(m/\epsilon)^{1/2}$] for the bulk and different film thickness: $D=5$ ($\approx 3.5R_g$; R_g is the bulk radius of gyration), $D=7$ ($\approx 5R_g$), $D=10$ ($\approx 7R_g$), and $D=20$ ($\approx 14R_g$). The critical temperatures were obtained from fits to Eq. (9) [see Table I]. The crossover time was determined from the mean-square displacement of the innermost monomer $g_1(t)$ by the condition $g_1(\tau_{co})=6r_{sc}^2=0.054$. This choice as well as power laws of both panels are motivated by a MCT analysis of the bulk data [40,50,51]. The value $6r_{sc}^2$ (roughly) coincides with the inflection point of $g_1(t)$ and thus marks the crossover from the early time regime, where $g_1(t)$ is almost flat, to the late time regime, where $g_1(t)$ increases faster with t and finally becomes diffusive [see Fig. 14]. The exponent a used to linearize the data close to T_c is that of the bulk ($a=0.352$ [40]).

$$g_1(t=\tau_{co}) := 6r_{sc}^2 = 0.054 \quad \text{(definition of } \tau_{co}\text{)}. \tag{14}$$

This definition is motivated by an analysis of the bulk, where r_{sc} ($\approx$ 0.1 monomer diameter) appears as a relevant length scale for the dynamics of a monomer in its local environment (''cage'') [40,50]. The value $6r_{sc}^2$ (roughly) coincides with the inflection point of $g_1(t)$ and thus marks the crossover from the early time regime, where $g_1(t)$ is almost flat, to the late time regime, where $g_1(t)$ gradually increases with time and finally becomes diffusive (see Fig. 14). Motivated by ideal MCT, one expects that τ_{co} diverges at T_c with a power law

$$\tau_{co}(T) \propto |T-T_c|^{-1/2a}, \tag{15}$$

with $0<a<0.5$. The exponent a describes the initial decay of the correlation functions from the ballistic regime to the plateau [12–14]. The analysis of the bulk data showed that $a=0.352$ [40].

Figure 13 displays τ_{co}^{-2a} versus $T-T_c$ for the bulk and for various film thicknesses: $D=5$ ($\approx 3.5R_g$; R_g is the bulk radius of gyration), $D=7$ ($\approx 5R_g$), $D=10$ ($\approx 7R_g$), and $D=20$ ($\approx 14R_g$). The critical temperatures are taken from Table I and for the exponent a we used the bulk value $a=0.352$ [40]. It is seen from Fig. 13 that this value yields a good linearization of the bulk data. For τ_{co} obtained from the film data, however, deviations occur indicating a (rather slight) D dependence of the exponent a.

The previous analysis of the T dependence of the relaxation time τ and of the crossover time τ_{co} suggests that the critical temperature depends strongly on film thickness, but the variation of the exponents a or γ is rather weak. Within the framework of MCT the exponents a and γ are related to one another and determined by the so-called exponent parameter λ, which controls the time evolution of the monomer mean-square displacement in the plateau regime (see Fig. 4). Thus, the weak variation of the exponents a and γ with D should imply that the time dependence of the mean-square displacements in the film closely follows that of the bulk, in the plateau regime. It is, therefore, interesting to test whether the mean-square displacements of the film and of the bulk obey the same master curve when compared for the same reduced temperature, $T-T_c$. This idea is first examined in the upper panel of Fig. 14 where the MSD's of the innermost monomers $g_1(t)$ and of the chain's center of mass $g_3(t)$ are compared at $T-T_c=0.07$ for the bulk and for a film of thickness $D=10$ (as $T_c^{\text{bulk}}=0.45$ and $T_c(D=10)=0.39$, the bulk data at $T=0.52$ are compared to the corresponding film data at $T=0.46$). There is a good agreement between the film and bulk data over a long period of time, in particular, for intermediate times. The lower panel of the figure extends this comparison to lower temperatures. Whereas the film data still closely agree with each other for all times simulated, this is no longer the case for the bulk data. By simply shifting the T axis it is only possible to rescale the bulk and film data onto a common master curve in the intermediate time window of the plateau. At later times, however, $g_1(t)$ of the bulk increases faster with t than $g_1(t)$ of the films. This difference is more pronounced the closer T is to $T_c(D)$.

A preliminary analysis of the incoherent scattering function also reveals the property that for intermediate times, the data corresponding to different film thicknesses follow the same master curve when compared for the same reduced temperature $T-T_c(D)$. A more detailed investigation and comparison with the behavior of the mean-square displacements is under way.

V. LOCAL DYNAMICS

The discussion of the preceding section illustrated that the dynamics of the film is accelerated with respect to the bulk. Obviously, this is a consequence of the walls. A natural question is, therefore, how the motion of the monomers depends on their distance from the wall. To obtain a better insight into this dependence we study the local displacements, i.e., the mean-square displacements measured within layers of a small thickness (bin) at various distances from the wall. However, when trying to analyze local displacements the problem of how to assign particles to layers has to be addressed. A possible definition is to associate a monomer labeled i to that bin to which its initial z position, $z_i(t_0)$, corresponds

$$g_0(t;z) = \left\langle \sum_{i=1}^{N} \delta(z-z_i(t_0)) \times [\mathbf{r}_i(t)-\mathbf{r}_i(t_0)]^2 \Big/ \sum_{1}^{N} \delta(z-z_i(t_0)) \right\rangle. \tag{16}$$

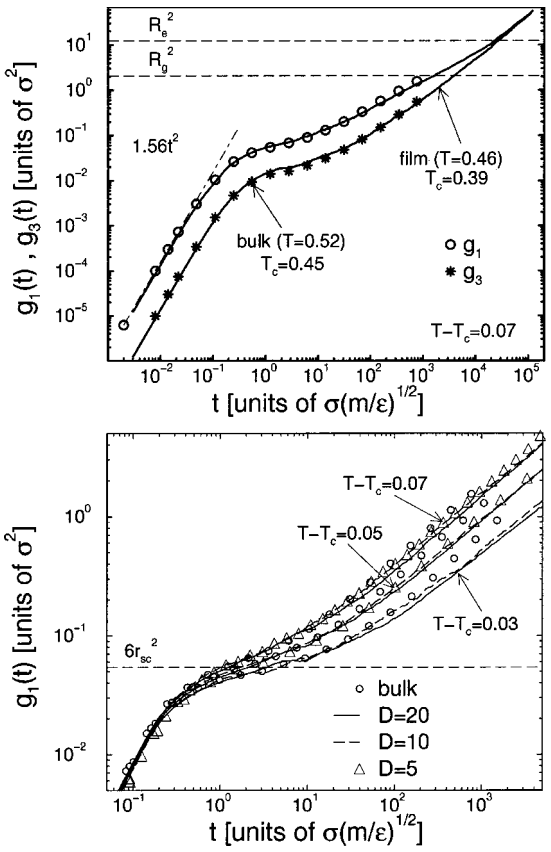

FIG. 14. Upper panel shows the mean-square displacements of the innermost monomer $g_1(t)$ and of the chain's center of mass $g_3(t)$ between the bulk (symbols ○ and ∗) and a film (solid lines) of thickness $D=10$ ($\approx 7R_g$). The panel compares the results for the same distance to the critical temperature T_c (i.e., $T-T_c=0.07$). The displacements of the film are calculated parallel to the wall. They were multiplied by $\frac{3}{2}$ to put them on the scale of the bulk data. The two horizontal dashed lines show the bulk end-to-end distance R_e^2 and the radius of gyration R_g^2, respectively. The ballistic short-time behavior $g_1(t)=3Tt^2$ is indicated for the bulk at $T=0.52$. The lower panel shows behavior of $g_1(t)$ for $D=5$, 10, 20, and for the bulk when approaching T_c [$T_c(D=5)=0.305$, $T_c(D=10)=0.39$, $T_c(D=20)=0.415$, $T_c^{\text{bulk}}=0.45$]. The dashed horizontal line shows the plateau value $6r_{\text{sc}}^2$ ($\simeq 0.054$) of a MCT analysis performed on the bulk data [40]. For intermediate times, the film and bulk data corresponding to a given $T-T_c$ follow the same master curve.

The drawback of this definition is, however, that some particles may leave this layer a later time. If one adds their contribution to the MSD to that of those particles that always remain in the initial region, a sort of averaging over other regions is introduced. Obviously, the larger the time difference $t-t_0$, the greater the probability that some tagged particle has left its initial layer. As a consequence, the local character of the obtained information becomes questionable for large times. An estimate of the time beyond which this averaging over neighboring regions becomes appreciable is the time at which the mean-square displacements in transverse direction become comparable to the half of the bin size. For larger times local information is gradually lost and the MSD's of different regions converge towards the average MSD of the whole system. This point is nicely demonstrated

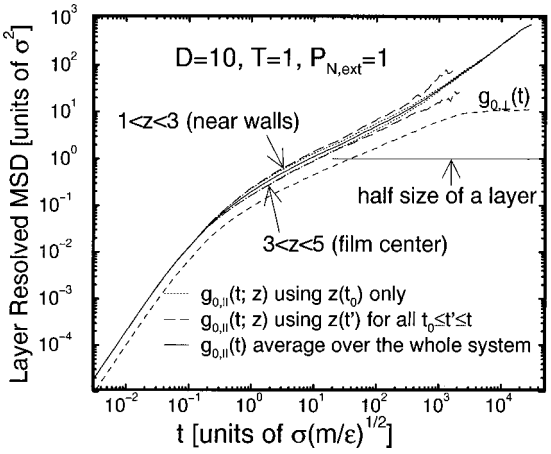

FIG. 15. Illustration of the dependence of the local MSD upon the way the particle displacements are attributed to layers (localized). For this purpose, two regions of different mobilities are considered: A region around the film center, $3 \le z \le 5$, and the first layer close to the walls, $1 \le z \le 3$ ($z=|z_{\text{particle}}-z_{\text{wall}}|$). Note that there is practically no particle in the very proximity of the walls, i.e., in the region with $0 \le z \le 1$. If the displacement of a particle is always attributed to the layer, where the particle was observed at t_0, the obtained results for the local MSD's are biased in the following sense: If a tagged particle leaves its initial layer at a later time, its motion will partly represent the properties of the layers it has ''visited'' so far. Attributing the mobility of such a particle to the initial layer thus represents an averaging over many layers. The error introduced in this way is negligible for short times. However, as the MSD in transverse direction $g_{0,\perp}(t)$ becomes comparable to the half of the layer thickness [see the intersection of the horizontal line with $g_{0,\perp}(t)$] the error dominates and the local character of the data is lost to a large extent. For very long times, no local information ''persists'' this averaging and curves belonging to different regions converge towards the system average [see long-time behavior of the dotted lines]. The correct definition requires that only those particles are allowed to contribute to the mobility of a given region, which stay in the same layer for all times $t_0 \le t' \le t$ [see long-dashed lines]. However, there is also a drawback to this correct definition: As any particle that leaves its initial layer must be excluded by the computation of the MSD's, the statistical uncertainty increases with the number of such particles and thus with time [see long-dashed lines for large t]. Statistical accuracy at large times thus requires more independent samples of the same system. The difference in the magnitude of $g_{0,\perp}(t)$ and $g_{0,\parallel}(t)$ arises from the fact that there is only one independent direction perpendicular to the walls compared to two independent parallel directions.

in Fig. 15 where the MSD of all monomers in the direction parallel to the walls $g_{0,\parallel}(t)$, is shown for two regions of different mobility in a film of thickness $D=10$ at $T=1$ (high temperature liquid state). As $g_{0,\parallel}>1$ (half of the bin size), the MSD of both regions converge towards that of the whole system for large times.

To avoid this problem, a more stringent criterion must be used to compute local MSD's from particle displacements: The contribution of a tagged particle to the MSD of a given layer at a time t should be taken into account if and only if the tagged particle has been in the same layer for *all times* $t_0 \le t' \le t$

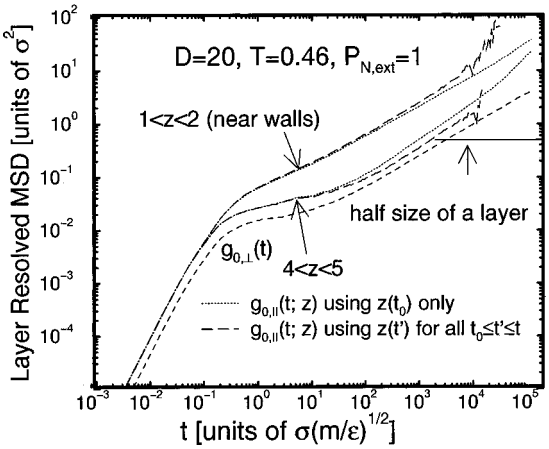

FIG. 16. Same as in Fig. 15 but for a film of thickness $D=20$ at a low temperature of $T=0.46$ [$T_c(D=20)=0.415$]. The figure illustrates that attributing the displacement of a particle to the layer, where it was at the initial time t_0, can lead to errors that strongly depend on the layer under consideration. Therefore, the results obtained using this definition are not reliable even at times for which the MSD in transverse direction $g_{0,\perp}$ is much smaller than the half of the layer thickness which, in turn, is the localization resolution. The difference in the magnitude of $g_{0,\perp}(t)$ and $g_{0,\|}(t)$ arises from the fact that there is only one independent direction perpendicular to the walls compared to two independent parallel directions.

$$g_0(t;z)=\left\langle \sum_{i=1}^{N}\prod_{t'=t_0}^{t}\delta(z-z'(t')) \times[\mathbf{r}_i(t)-\mathbf{r}_i(t_0)]^2 \Big/ \sum_{1}^{N}\prod_{t'=t_0}^{t}\delta(z-z_i(t'))\right\rangle. \tag{17}$$

This correct definition is, however, computationally more demanding. The reason lies in the fact that the contribution of particles, which have left their initial layer at some later time, has to be ignored for all subsequent times. As the number of such particles increases with time, the statistical accuracy decreases at late times. To improve it, one needs more independent samples of the same system.

In Fig. 16 we focus on another aspect of the same problem. Figure 15 suggests that a good estimate of the time at which the difference between Eqs. (16) and (17) is no longer negligible is $g_{1,\|}(t)=(\text{bin width})/2$. Here, we stress that the inverse is not necessarily true, i.e., the error is not necessarily negligible for shorter times. Already in Fig. 15 one can observe that, in the case of the layer close to the wall, deviations from the correct curve occur at shorter times than the intersection point between $g_{0,\perp}(t)$ and the horizontal line indicating half of the layer thickness. This point is more clearly demonstrated in Fig. 16 where the MSD's of a film of thickness $D=20$ at a low temperature of $T=0.46$ are used [$T_c(D=20)=0.415$]. Here, for the layer in the inner part of the system, the deviations are appreciable already at times, which are about two orders of magnitude smaller than the ''intersection time.'' One should, therefore, be aware of this discrepancy when analyzing local quantities.

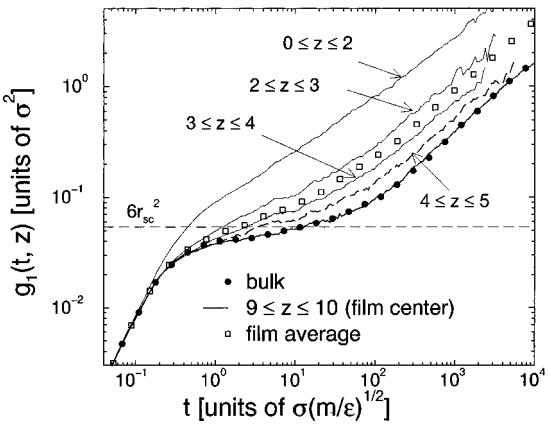

FIG. 17. Layer-resolved mean-square displacement of the innermost monomer $g_1(z,t)$ versus time for a film of thickness $D=20$ ($\approx 14R_g$; R_g is the bulk radius of gyration) at $T=0.46$ ($T_c(D=20)=0.415$; see Table I). z denotes the distance from the (left) wall. The displacements are calculated parallel to the wall and multiplied by $\frac{3}{2}$ (to put them on the same scale as the bulk data (●) which are averaged over three spatial dimensions instead of over only two for the film). The $g_1(z,t)$ data (indicated by lines) are averages over all mononiers between some $z_{\min}\leqslant z\leqslant z_{\max}$ which remain in the specified z interval for all times shown in the figure. Due to the loss of the statistical accuracy at late times, the data are some times cut off at times with large statistical noise. In the middle of the film ($9\leqslant z\leqslant 10$) $g_1(z,t)$ coincides with $g_1(t)$ of the bulk, whereas it is much faster at the wall ($0\leqslant z\leqslant 2$). The average behavior of the film (i.e., the average over all layers) is shown by □. The dashed horizontal line indicates the plateau value $6r_{sc}^2$ ($\simeq 0.054$) of a MCT analysis performed in the bulk [40,50,51].

Figure 17 depicts the local MSD of the innermost monomer, $g_1(t;z)$, for a film of thickness $D=20$ at a low temperature of $T=0.46$. The displacements are calculated parallel to the walls using Eq. (17). We see from this figure that the mobility in film center is practically equal to that of the bulk, whereas monomers in the proximity of the wall are much more mobile. There is a gradual transition from the two step relaxation characteristic of the bulk at this temperature to a smooth crossover from microscopic to free diffusive motion as the layers are closer to the wall. Whereas the bulk-like dynamics for the film center is plausible—the monomer density profile is flat there and equal to ρ_{bulk} (see Fig. 19), the continuous speeding up of the dynamics in spite of the pronounced oscillations of the monomer density is less intuitive. It could be related to the following points: An important factor is certainly the wall potential. This potential is softer [see Eq. (2)] than the *LJ* potential that means that a monomer close to a wall can further penetrate the wall than a monomer can approach the center of mass of its nearest neighbors. This should yield a higher mobility of the monomers at the wall at low T where the dense local packing of the monomers is responsible for the mutual blocking and slowing down of the bulk dynamics.

On the other hand, the static structure factor of Fig. 1 shows that the first maximum is not as large in the film as in the bulk at the same low temperature. This implies that the overall arrangement of the monomers in the nearest neighbor

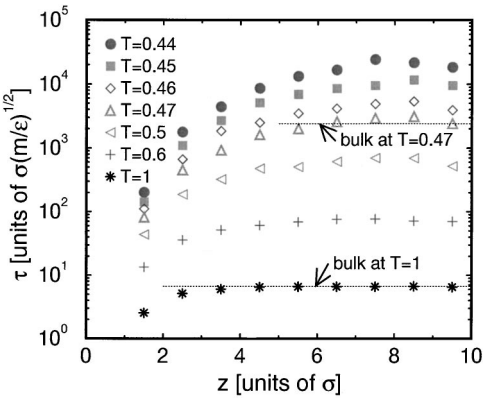

FIG. 18. Relaxation time $\tau(g_0=1;z)$ versus distance from the wall for a film of thickness $D=20$ ($\approx 14R_g$; R_g is the bulk radius of gyration). Here, z stands for the distance of the center of a layer (bin) from the (left) wall. The thickness of a bin is $\Delta z=1$. In the calculation of the local mean-square displacements of all monomers, $g_0(t,z)$, which underlies the definition of τ, we consider the contribution of only those monomers, which remain within the specified layer for all times $t' \leqslant t$ (see also the text). At high temperatures, there is a wide region around the film center, where τ is independent of z. Contrary to that, at low T, the presence of the walls is ''felt'' also close to the film center [note that the lowest temperature is close to $T_c(D=20)=0.415$; see Table I].

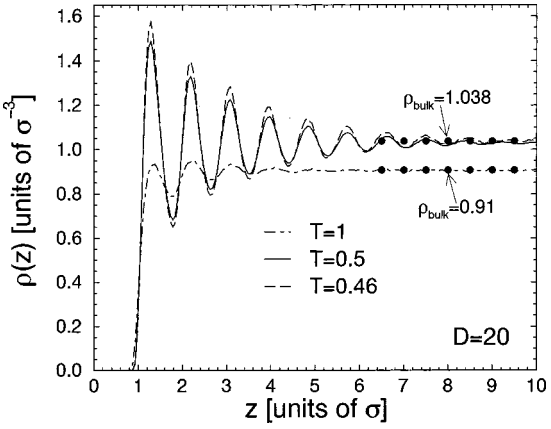

FIG. 19. Temperature dependence of the monomer density profile $\rho(z)$ for $D=20\approx 14R_g$ (R_g is the bulk radius of gyration). z denotes the position of a monomer from the (left) wall. Since the profiles are symmetric with respect to the middle of the film, only one half is shown. The temperatures are characteristic of the high-temperature state ($T=1$) and the supercooled state ($T=0.46 > T_c(20)=0.415$; see Table I) of the melt. The horizontal filled circles (●) indicate the bulk densities $\rho_{\text{bulk}}=0.91$ and $\rho_{\text{bulk}}=1.038$ at $T=1$ and $T=0.46$, respectively.

shells is not as pronounced in the direction parallel to the wall as it is in the bulk. Since this local packing is an important factor for the slowing down of the structural relaxation (Hansen-Verlet freezing criterion), the dynamics in the film should be faster.

Using a local version of Eq. (6), we define a z-dependent relaxation time $\tau(z)$

$$g_i(t=\tau(z);z) := 1 \quad \text{[defining equation for } \tau(z)\text{]}, \quad (18)$$

where $i=0$, 1, 3, 4 denotes various types of displacements of a polymer system (see Sec. III and IV).

For a film of thickness $D=20$, we applied Eq. (18) to the local MSD of all monomers, $g_0(t;z)$, and computed $\tau(z)$ at various temperatures. The results thus obtained are displayed in Fig. 18. Not unexpectedly, the effect of the walls is quite small at high temperatures. At $T=1$, for example, there is a wide region of z-independent relaxation time around the film center. This constant value agrees with the relaxation time τ obtained by applying Eq. (6) to the bulk data. As the temperature decreases the presence of the walls is ''felt'' also in the inner part of the film and the width of the region of the constant relaxation time decreases.

This propagation of the wall effects into the inner part of the film is also observed in the density profile. Figure 19 shows that density oscillations become more pronounced and long ranged at lower temperatures. Since the normal pressure is kept constant during the simulations (as it was also the case in preceeding simulations in the bulk [40]), the average value of the density in the film center increases with decreasing temperature and coincides with that of the bulk at the same temperature. This increase of the density in the film gives rise to more pronounced oscillations of the monomer profile.

VI. CONCLUSION

We presented results on molecular-dynamics simulations for a model of nonentangled short polymer chains confined between two perfectly flat, nonadsorbing and impenetrable walls. The monomer-wall interaction is modeled by a potential that diverges as z^{-9} when a monomer approaches the wall. This repulsion is weaker than the 12-6 Lennard-Jones potential of the monomer-monomer interaction and also than the soft-sphere potential ($\sim z^{-12}$) used in simulations of confined supercooled simple liquids [54,55]. This special choice of the monomer-wall interaction has an influence on both the static and dynamic properties of the polymer films.

We find oscillations of the monomer density that start from a large value close to the wall and decay towards the bulk density in the middle of the film for sufficiently large film thickness. The amplitude of these oscillations becomes more pronounced with the decreasing temperature, since the bulk density increases in our constant-pressure simulations. However, the height of the largest maximum at the wall does not exceed 1.5 times the bulk density in the temperature range studied. This is much smaller than the difference found in simulations where the particle-wall interaction is modeled by a soft-sphere potential. There, the density can be more than four times larger than the bulk density at low T, which leads to a vanishing of the density in the subsequent minimum. In this case it is conceivable that the smoothness of the walls, which could promote fast particle motion (slip boundary condition), is completely outweighed by the high density in the first layer, and one can speculate that the subsequent layers are also slowed down with respect to the bulk. This

could explain why the studies [54,55] found an increase of the glass transition temperature rather than a decrease although the confinement was realized by completely smooth walls as in our work.

In our work the repulsive monomer-wall interaction is much softer, even than that between the monomers in the bulk. Therefore, a monomer can come closer to the wall than to anyone of its nearest neighbors. This should give a monomer at the wall more freedom to move. Since the slowing down of the structural relaxation of our model in the bulk mainly results from the blocking of a particle by its nearest neighbors [40,50,51], one can expect this difference in repulsive interaction to become particularly important at low temperatures close to T_c. This expectation is borne out by the simulation data. Whereas the monomers in the film center exhibit very sluggish motion in an intermediate time interval, a signature of the ''cage effect,'' this intermittence of the displacements is not at all visible for the monomers in contact with the wall. They behave as if they were at a higher temperature (see Fig. 17). Their higher mobility also triggers faster motion of adjacent monomers, leading to an overall acceleration of the dynamics in the film.

We have tried to quantify this acceleration by fitting various relaxation times and the diffusion coefficient of a chain to both a power law, motivated by mode coupling theory (MCT), and by the Vogel-Fulcher-Tammann (VFT) equation. The power law yields an estimate of the critical temperature T_c and the VFT equation of the Vogel-Fulcher temperature T_0 as a function of film thickness D. In accord with the qualitative observations described above both $T_c(D)$ and $T_0(D)$ decrease with decreasing film thickness. Furthermore, a comparison of the rescaled quantities, i.e., of $T_c(D)/T_c^{\mathrm{bulk}}$ and $T_0(D)/T_0^{\mathrm{bulk}}$, shows that the variation with D of $T_c(D)$ agrees with that of $T_0(D)$. Although the extrapolation to T_0 is less reliable than that to T_c, since it has to cover a larger T range, this result suggests that the glass transition temperature of our model should follow the same behavior.

The reduction of the critical temperature seems to be the dominant influence of the walls on the dynamics in the time window of the MCT-β process. For these intermediate times, the mean-square displacements of the films of various thicknesses and of the bulk exhibit the same time dependence when compared for a fixed reduced temperature $T-T_c$. This shifting property of the temperature axis suggests that similar processes cause the intermittence of monomer motion on these intermediate time scales in the bulk and in the films. However, deviations between film and bulk dynamics are found as soon as the monomers escape from their local environment and the α relaxation sets in. In order to understand these differences better we want to investigate the incoherent intermediate scattering function and related quantities that provide information on the dynamics on different length scales. Work in this direction is under way.

ACKNOWLEDGMENT

We thank J. Horbach, P. Scheidler, C. Brangian, and M. Aichele for helpful discussions on various aspects of this work. We gratefully acknowledge the financial support of the ''Deutsche Forschungsgemeinschaft'' (DFG) under the Project No. SFB262 and by Bundesministerium für Bildung und Forschung (BMBF). We are also indebted to the European Science Foundation for financial support by the ESF Program on ''Experimental and Theoretical Investigations of Complex Polymer Structures'' (SUPERNET). Generous grants of simulation time by the computer center at the University of Mainz (Z.D.V.), the NIC in Jülich, and the RHRK in Kaiserslautern are also acknowledged.

[1] X. Zhang and J. Bell, Polym. Eng. Sci. **39**, 119 (1999).
[2] J. Rayss, W. Podkoscielny, and J. Widomski, J. Appl. Polym. Sci. **49**, 835 (1993).
[3] R. Armstrong and D. Wright, Electrochim. Acta **38**, 1799 (1993).
[4] M. Cohen and G. Grest, Phys. Rev. B **20**, 1077 (1979).
[5] M. Cohen and D. Turnbull, J. Chem. Phys. **31**, 1164 (1959).
[6] M. Cohen and D. Turnbull, J. Chem. Phys. **34**, 120 (1961).
[7] M. Cohen and D. Turnbull, J. Chem. Phys. **52**, 3038 (1970).
[8] J. Gibbs and E. DiMarzio, J. Chem. Phys. **28**, 373 (1958).
[9] J. Gibbs and E. DiMarzio, J. Chem. Phys. **28**, 807 (1958).
[10] U. Bengtzelius, W. Götze, and A. Sjölander, J. Phys. C **17**, 59 115 (1984).
[11] W. Götze, in *Proceedings of the Les Houches Summer School, 1989, Session LI*, edited by J. Hansen, D. Levesque, and J. Zinn-Justin (North-Holland, Amsterdam, 1989), pp. 287–503.
[12] W. Götze, in *Liquids*, edited by J. Hansen, D. Levesque, and Zinn-Justin (North-Holland, Amsterdam, 1991), p. 287.
[13] W. Götze and L. Sjögren, Transp. Theory Stat. Phys. **24**, 801 (1995).
[14] W. Götze and L. Sjögren, Rep. Prog. Phys. **55**, 241 (1992).
[15] W. Kob, in *Annual Review of Computational Physics*, edited by D. Stauffer (World Scientific, Singapore, 1995).
[16] G. Adam and J. Gibbs, J. Chem. Phys. **43**, 139 (1965).
[17] P. Chaikin and T. Lubensky, *Principles of Condesed Matter Physics* (Cambridge University Press, Cambridge, 1995).
[18] S. Edwards and T. Vilgis, Phys. Scr., T **T13**, 7 (1986).
[19] W. Kob *et al.*, Phys. Rev. Lett. **79**, 2827 (1997).
[20] C. Donati *et al.*, Phys. Rev. E **60**, 3107 (1999).
[21] C. Bennemann, C. Donati, J. Baschnagel, and S. Glotzer, Nature (London) **399**, 246 (1999).
[22] R. Yamamoto and A. Onuki, Phys. Rev. E **58**, 3515 (1998).
[23] R. Yamamoto and A. Onuki, J. Phys. Soc. Jpn. **66**, 2545 (1997).
[24] R. Yamamoto and A. Onuki, Europhys. Lett. **40**, 61 (1997).
[25] A. Onuki and R. Yamamoto, J. Non-Cryst. Solids **235-237**, 34 (1998).
[26] J. Forrest and J. Mattsson, Phys. Rev. E **61**, R53 (2000).
[27] P. Ray and K. Binder, Europhys. Lett. **27**, 53 (1994).
[28] J. Keddie, R. Jones, and R. Cory, Faraday Discuss. **98**, 219 (1994).
[29] J. Keddie, R. Jones, and R. Cory, Europhys. Lett. **27**, 59 (1994).

[30] J. Forrest, K. Dalnoki-Veress, J. Stevens, and J. Dutcher, Phys. Rev. Lett. **77**, 4108 (1996).
[31] J. Forrest, K. Dalnoki-Veress, J. Stevens, and J. Dutcher, Phys. Rev. Lett. **77**, 2002 (1996).
[32] J. Forrest and R. Jones, in *Polymer Surfaces, Interfaces and Thin Films*, edited by A. Karim and S. Kumar (World Scientific, Singapore, 2000), pp. 251–294.
[33] J. Forrest, K. Dalnoki-Veress, and J. Dutcher, Phys. Rev. E **56**, 5705 (1997).
[34] P. de Gennes, Eur. Phys. J. E **2**, 201 (2000).
[35] J. Torres, P. Nealey, and J. de Pablo, Phys. Rev. Lett. **85**, 3221 (2000).
[36] F. Varnik, J. Baschnagel, and K. Binder, J. Phys. IV **10**, 239 (2000).
[37] F. Varnik, J. Baschnagel, and K. Binder, J. Chem. Phys. **113**, 4444 (2000).
[38] K. Kremer and G. Grest, J. Chem. Phys. **92**, 5057 (1990).
[39] C. Bennemann, W. Paul, K. Binder, and B. Dünweg, Phys. Rev. E **57**, 843 (1998).
[40] C. Bennemann, J. Baschnagel, and W. Paul, Eur. Phys. J. B **10**, 323 (1999).
[41] F. Varnik, J. Baschnagel, and K. Binder (unpublished).
[42] S. Nosé, J. Chem. Phys. **81**, 511 (1984).
[43] W. Hoover, Phys. Rev. A **31**, 1695 (1985).
[44] F. Varnik, Ph.D. thesis, University of Mainz, 2000; available at http://ArchiMeD.uni-mainz.de/pub/2001/0007/
[45] S. Nosé and M. Klein, Mol. Phys. **50**, 1055 (1983).
[46] W. Hoover, A. Ladd, and B. Moran, Phys. Rev. Lett. **48**, 1818 (1982).
[47] W. Hoover, Phys. Rev. A **34**, 2499 (1986).
[48] S. Nosé, Mol. Phys. **52**, 255 (1984).
[49] P. Rouse, J. Chem. Phys. **21**, 1272 (1953).
[50] M. Aichele and J. Baschnagel, Eur. Phys. J. E **5**, 229 (2001).
[51] M. Aichele and J. Baschnagel, Eur. Phys. J. E **5**, 245 (2001).
[52] C. Bennemann, J. Baschnagel, W. Paul, and K. Binder, Comput. Theor. Polym. Sci. **9**, 217 (1999).
[53] K. Dalnoki-Veress *et al.*, Phys. Rev. E **63**, 31 801 (2001).
[54] R. Yamamoto and K. Kim, J. Phys. IV **10**, 15 (2000).
[55] T. Fehr and H. Löwen, Phys. Rev. E **52**, 4016 (1995).